

# Terahertz radiation shaping based on optical spectrum modulation in the time domain

Jesús Palací,\* Alexander Bockelt, and Borja Vidal

Valencia Nanophotonics Technology Center, Universidad Politécnica de Valencia, Camino de Vera s/n 46022, Valencia, Spain

\*jespalpe@gmail.com

**Abstract:** A terahertz shaping system based on optical fiber components as opposed to traditional free-space solutions is proposed. It is based on the time-domain modulation of the optical source spectrum. Standard single-mode fiber distributes and disperses the pulse before filtering its spectral components by means of the cross-gain and cross-phase modulation effects taking place in an interferometric semiconductor optical amplifier structure. Experimental measurements are obtained, showing the tunability of the system as well as its reconfigurability.

©2012 Optical Society of America

**OCIS codes:** (300.0300)\_Spectroscopy; (040.2235) Far infrared or terahertz; (160.5140) Photoconductive materials; (190.4370) Nonlinear optics, fibers.

---

## References and links

1. P. H. Siegel, "Terahertz technology," *IEEE Trans. Microw. Theory Tech.* **50**(3), 910–928 (2002).
2. J. Faist, F. Capasso, D. L. Sivco, C. Sirtori, A. L. Hutchinson, and A. Y. Cho, "Quantum cascade laser," *Science* **264**(5158), 553–556 (1994).
3. Y.-S. Lee, T. Meade, V. Perlin, H. Winful, T. B. Norris, and A. Galvanauskas, "Generation of narrow-band terahertz radiation via optical rectification of femtosecond pulses in periodically poled lithium niobate," *Appl. Phys. Lett.* **76**(18), 2505–2507 (2000).
4. Q. Wu and X.-C. Zhang, "Free-space electro-optic sampling of terahertz beams," *Appl. Phys. Lett.* **67**(24), 3523–3525 (1995).
5. D. H. Auston, K. P. Cheung, J. A. Valdmanis, and D. A. Kleinman, "Cherenkov radiation from femtosecond optical pulses in electro-optic media," *Phys. Rev. Lett.* **53**(16), 1555–1558 (1984).
6. D. H. Auston, K. P. Cheung, and P. R. Smith, "Picosecond photoconducting Hertzian dipoles," *Appl. Phys. Lett.* **45**(3), 284–286 (1984).
7. N. Chimot, J. Mangeney, L. Joulaud, P. Crozat, H. Bernas, K. Blary, and J. F. Lampin, "Terahertz radiation from heavy-ion-irradiated  $\text{In}_{0.53}\text{Ga}_{0.47}\text{As}$  photoconductive antenna excited at 1.55  $\mu\text{m}$ ," *Appl. Phys. Lett.* **87**(19), 193510 (2005).
8. A. M. Weiner, "Ultrafast optical pulse shaping: a tutorial review," *Opt. Commun.* **284**(15), 3669–3692 (2011).
9. Y. Liu, S.-G. Park, and A. M. Weiner, "Terahertz waveform synthesis via optical pulse shaping," *IEEE J. Sel. Top. Quantum Electron.* **2**(3), 709–719 (1996).
10. J. Y. Sohn, Y. H. Ahn, D. J. Park, E. Oh, and D. S. Kim, "Tunable terahertz generation using femtosecond pulse shaping," *Appl. Phys. Lett.* **81**(1), 13–15 (2002).
11. A. M. Weiner, "Femtosecond pulse shaping using spatial light modulators," *Rev. Sci. Instrum.* **71**(5), 1929–1960 (2000).
12. R. J. B. Dietz, M. Gerhard, D. Stanze, M. Koch, B. Sartorius, and M. Schell, "THz generation at 1.55  $\mu\text{m}$  excitation: six-fold increase in THz conversion efficiency by separated photoconductive and trapping regions," *Opt. Express* **19**(27), 25911–25917 (2011).
13. J. R. Middendorf and E. R. Brown, "THz generation using extrinsic photoconductivity at 1550 nm," *Opt. Express* **20**(15), 16504–16509 (2012).
14. A. S. Weling and D. H. Auston, "Novel sources and detectors for coherent tunable narrow-band terahertz radiation in free space," *J. Opt. Soc. Am. B* **13**(12), 2783–2791 (1996).
15. J. Palací and B. Vidal, "Tunable and reconfigurable narrow-band THz generation using photoconductive antennas and chirped-pulse mixing," in *Proceedings of the International Topical Meeting on Microwave Photonics* (Singapore, 2011), pp. 210–213.
16. R. E. Saperstein, N. Alic, D. Panasenko, R. Rokitski, and Y. Fainman, "Time-domain waveform processing by chromatic dispersion for temporal shaping of optical pulses," *J. Opt. Soc. Am. B* **22**(11), 2427–2436 (2005).
17. H. Ju, S. Zhang, D. Lenstra, H. de Waardt, E. Tangdiongga, G. Khoe, and H. Dorren, "SOA-based all-optical switch with subpicosecond full recovery," *Opt. Express* **13**(3), 942–947 (2005).
18. A. J. Zilkie, J. Meier, M. Mojahedi, P. J. Poole, P. Barrios, D. Poitras, T. J. Rotter, C. Yang, A. Stintz, K. J. Malloy, P. W. E. Smith, and J. S. Aitchison, "Carrier dynamics of quantum-dot, quantum-dash, and quantum-

- well semiconductor optical amplifiers operating at 1.55  $\mu\text{m}$ ," *IEEE J. Quantum Electron.* **43**(11), 982–991 (2007).
19. A. S. Weling and T. F. Heinz, "Enhancement in the spectral irradiance of photoconducting terahertz emitters by chirped-pulse mixing," *J. Opt. Soc. Am. B* **16**(9), 1455–1467 (1999).
  20. R. Inohara, K. Nishimura, M. Tsurusawa, and M. Usami, "Experimental analysis of cross-phase modulation and cross-gain modulation in SOA-injecting CW assist light," *IEEE Photon. Technol. Lett.* **15**(9), 1192–1194 (2003).
  21. A. J. Lowery, "New dynamic semiconductor laser model based on the transmission line modeling method," *IEEE Proc. J. Optoelectron.* **134**(5), 281–289 (1987).
  22. A. I. Siahlo, A. T. Clausen, L. K. Oxenløwe, J. Seoane, K. S. Berg, Z. Xu, J. Zeng, and P. Jeppesen, "Phase modulation for postcompensation of dispersion in 160 Gb/s systems," *IEEE Photon. Technol. Lett.* **17**(2), 498–500 (2005).</jrn>
- 

## 1. Introduction

Submillimeter radiation shows a great potential in a wide range of fields from imaging and material identification to biology and communications [1]. However the generation and detection in this frequency band remains difficult. Electronic commercial solutions are available up to a few hundreds of GHz while quantum-cascade lasers (QCLs) [2] are suitable for frequencies over 1 THz although cryogenic operation prevents wide application.

Photonic schemes require an optical source but they are easy to operate, more flexible and able to cover most of the THz gap. Among the different photonic solutions, such as periodically poled lithium niobate (PPLN) [3], electro-optic sampling using different crystals [4] or Cherenkov radiation [5], photoconductive antennas (PCAs) [6] are widely employed. PCAs, usually fed by Ti:Sapphire lasers, are key components in THz time-domain spectroscopy (THz-TDS) systems. Recently new commercial PCA designs with lower energy gaps that can be excited with 1.5  $\mu\text{m}$  light have reached the market [7]. Therefore cheaper optical sources developed for the telecommunication industry can be employed as well as other devices like Erbium-doped fiber amplifiers (EDFAs), electro-optic modulators (EOMs), semiconductor optical amplifiers (SOAs) and single-mode and specialty optical fibers for signal distribution and processing.

The processing of ultra-short optical pulses has been extensively studied due to its applicability in different areas [8]. Most of the proposed solutions are based on the direct control of the optical spectrum of the pulses. Typically, the different components are spatially separated using diffractive elements as gratings, before a phase/amplitude spatial modulation is applied on the different spectral components by means of phase masks [9], reconfigurable metallic structures [10] or spatial light modulators [11]. The latter provides much more flexibility enabling the implementation of quasi-arbitrary waveforms. However free-space components are susceptible of misalignment, long-term stability problems and result in bulky systems. On the other hand, the recent increase in the performance of THz sources excited with 1.5  $\mu\text{m}$  sources [12,13] motivates research for fiber-based processing of ultra-short pulses with applicability to the THz band. Recently, a technique based on the optical heterodyning of a time-stretched ultra-short optical pulse with its delayed replica to generate narrow-band THz radiation [14] has been demonstrated using fiber-based components [15]. Despite of its good performance and simplicity, the bandwidth of the generated radiation is related to its central frequency, limiting the flexibility of the system. Another approach which has been applied to the microwave range relies on the time-domain modulation of the optical spectrum, obtaining high time-bandwidth products and providing accurate control over the generated waveforms [16]. In this architecture optical fiber is employed as the dispersive medium and EOMs shape the time-decomposed spectrum. Thus the performance of the setup is limited by the stretched pulse duration and the modulator speed, which rarely exceeds a few tens of GHz.

SOAs have been traditionally employed for applications requiring short time responses like optical switching [17]. Particularly, multiple quantum well (MQW) optical amplifiers show short-term amplitude and phase dynamics below the ps [18], which makes them suitable for most ultrafast applications.

The generation of certain terahertz waveforms to concentrate the radiation into a given frequency band locally raises the energy density and therefore increases the dynamic range of

the system at those frequencies [19]. In this work an all-fiber all-optical dynamically-controlled THz pulse shaper is proposed and demonstrated. It is based on processing the optical source in a SOA Mach-Zehnder interferometer (SOA-MZI). The different spectral components are shaped in the time domain employing the cross-gain (XGM) and cross-phase modulation (XPM) effects taking place in the SOA-MZI. Experimental measurements have been performed validating the feasibility of the technique as well as the tunability of the THz central frequency and its bandwidth.

## 2. Principle of operation

The proposed technique is based on shaping the spectrum of a pulsed source by changing the interference conditions of an SOA-MZI in which the time-stretched pulses have been injected. Thanks to the fast response of this structure it is possible to separately modulate the different spectral components.

Figure 1(a) shows the schematic of the SOA-MZI as well as the interference experienced by an optical pulse entering the structure. The optical pulse is injected into both SOAs by means of several integrated optical couplers. Pulses in both branches of the interferometer are amplified by their respective SOA experiencing amplitude and spectral phase changes according to the bias current injected to the amplifiers. The output stage is symmetric with respect to the input and combines the pulses. Constructive or destructive interference occurs for the phase conditions shown.

Consider the scenario of Fig. 1(b). An optical pulse to be shaped is linearly chirped and injected into the SOA-MZI. An optical waveform used to control the shaping of the previous pulse counter-propagates through the upper SOA. Assuming that the shaping waveform is a single optical pulse with a duration much shorter than the recovery time of SOA<sub>1</sub>,  $\tau_{rec}$ , and that the gain response of SOA<sub>1</sub> follows a negative exponential as in [20], the electrical fields at the output of the SOAs are given by

$$E_{SOA_1}^{out}(t) = \sqrt{I_{SOA_1}(1 - \alpha_{XGM} \cdot \exp(-t / \tau_{rec}))} \exp\left(j\left(\varphi_{SOA_1} + \varphi_{XPM} \cdot \exp(-t / \tau_{rec})\right)\right) \quad (1)$$

$$E_{SOA_2}^{out}(t) = \sqrt{I_{SOA_2}} \exp(j\varphi_{SOA_2}) \exp(j\pi) \quad (2)$$

being  $I_{SOA_1}$  and  $I_{SOA_2}$  the average power at the output of the SOAs,  $\alpha_{XGM}$  a factor that measures SOA<sub>1</sub> gain reduction due to gain saturation when the short pulse arrives,  $\varphi_{SOA_1}$  and  $\varphi_{SOA_2}$  the phase shifts introduced by the SOAs onto the chirped pulse and  $\varphi_{XPM}$  the maximum phase shift originated by XPM. The last exponential of Eq. (2) is for the  $\pi$  phase shift introduced by the optical couplers in SOA<sub>2</sub> with respect to SOA<sub>1</sub>. The electrical fields combine by means of the output couplers of the MZI structure and an optical power at the output of the system proportional to  $\left|E_{SOA_1}^{out}(t) + E_{SOA_2}^{out}(t)\right|^2$  is obtained.

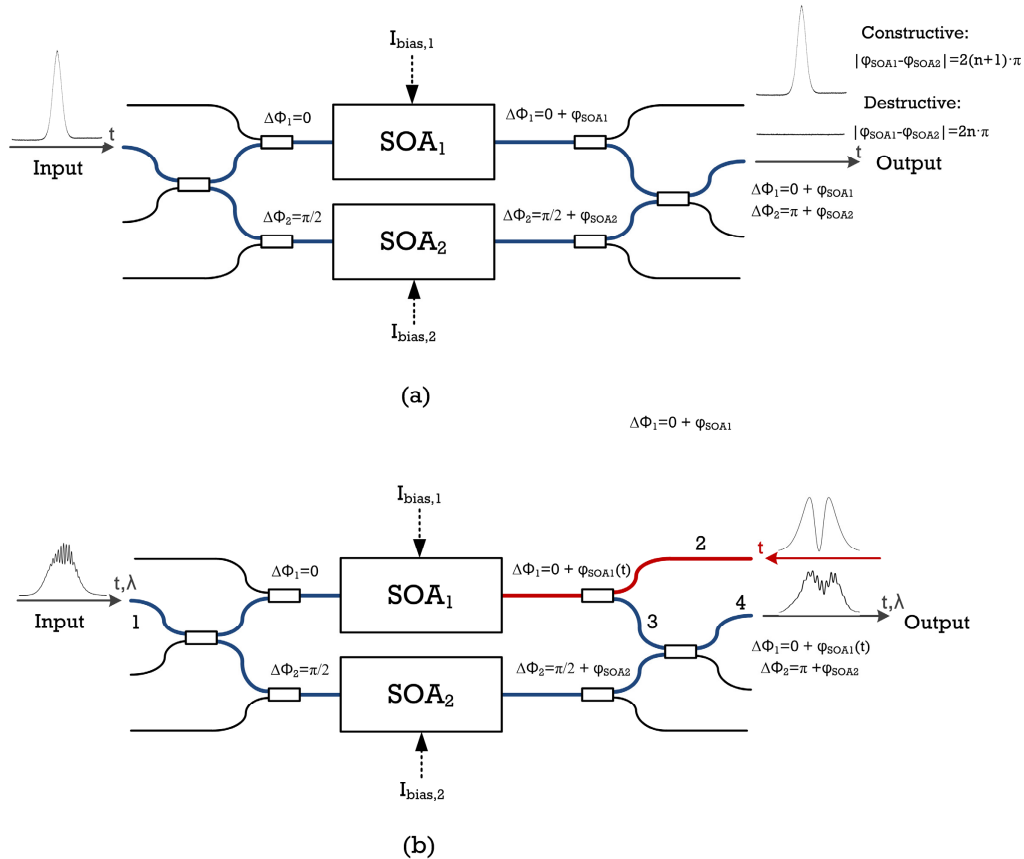


Fig. 1. (a) SOA interferometer block diagram. (b) SOA interferometer considering a chirped pulse and an additional counter-propagating pulse.

In the initial state,  $t < 0$ , no external pulse is injected into the system. Assuming identical SOAs, when the same biasing currents  $I_{bias}$  are applied to both devices  $I_{SOA_1}$  equals  $I_{SOA_2}$  as well as  $\varphi_{SOA_1}$  with respect to  $\varphi_{SOA_2}$ . Thus, the chirped pulse is suppressed. However, the arrival at  $t = 0$  of a pulse with enough energy to reduce the carrier density of  $SOA_1$  will temporarily change its gain and phase profiles through the  $\alpha_{XGM}$  and  $\varphi_{XPM}$  parameters, putting the system out of the destructive state and impressing variations onto the chirped pulse (i.e. performing an all-optical pulse shaper at the output of port 4). The transform-limited version of the shaped spectrum is obtained after compensating for the initial chirp.

### 3. Experimental results

Figure 2 shows the THz-TDS architecture. Gaussian-shaped optical pulses are generated in a femtosecond fiber-laser (fs-FL) with an average power of 5 dBm at a 50 MHz repetition rate and an estimated full-width at half maximum (FWHM) duration of 100 fs. These pulses are time-stretched by means of 4.16 km of dispersion compensation fiber (DCF) with a dispersion parameter ( $D$ ) of  $-100$  ps/km·nm and a dispersion slope ( $S$ ) of  $0.08$  ps/km·nm<sup>2</sup>. Thus, the pulses suffer a total dispersion ( $D_T$ ) of  $-416$  ps/nm with a slope of  $0.33$  ps/nm<sup>2</sup>. By using DCF as the dispersive medium, with a much higher dispersion parameter to that of standard single-mode fiber (SSMF) and a similar dispersion slope, the influence of the dispersion slope on the system performance becomes low enough to be neglected.

A polarization controller (PC) is included at the input of the SOA-MZI to account for the polarization dependence of the interferometric structure. The SOA-MZI, manufactured by CIP, comprises two identical bulk SOAs and a set of optical couplers with a 3 dB splitting ratio to form an interferometer. A transmission-line model technique was applied to model the SOAs according to [21]. The length of both SOAs is 500  $\mu\text{m}$  with a linewidth enhancement factor of 8, a noise figure of 8 dB, a confinement factor of 0.3 and a spontaneous emission factor of 1.5. The transparency current is estimated to be 17 mA and the unsaturated fiber-to-fiber gain is 13 dB. Carrier lifetimes of 1 ns and 300 ps were measured under 100 and 250 mA biasing, respectively.

The optical waveform used to control the SOA-MZI (shaping waveform) is derived from the same source than the pulses to be shaped. In this case a fiber Mach-Zehnder interferometer (MZI) was implemented using an optical delay line (ODL) to introduce a delay difference between its arms of  $\tau_{\text{ODL}}$  and select two spectral bands of the chirped pulse. SSMF with a length of  $L$  was included for pulse widening. Since two bands are filtered a train of pulses with repetition frequency  $f_{\text{rep}}$  is obtained after compensation for the initial chirp. Its value is related to the different parameters of the system as follows.

$$f_{\text{rep}} \approx \frac{\tau_{\text{ODL}}}{|D_T|} \quad (3)$$

The effect of the dispersion slope has been neglected due to its low influence. Regarding the temporal response of the SOA-MZI structure, for shaping waveforms much shorter than the gain recovery time of the SOAs the bandwidth of the filtered bands is given by the recovery time of the SOA while for longer ones the filtered bands approximately follow the shaping waveform. From now on the variable  $\tau_{\text{system}}$  is used for the FWHM duration of the system response to an arbitrary shaping pulse width. The FWHM bandwidth of the filtered spectrum  $\Delta\nu$  can be expressed as

$$\Delta\nu \approx \frac{\tau_{\text{system}}}{|D_T|} \quad (4)$$

The FWHM duration of the pulse train envelope can be expressed in terms of the time-bandwidth product (TBP) and Eq. (4) as

$$\Delta\tau \approx \frac{\text{TBP}|D_T|}{\tau_{\text{system}}} \quad (5)$$

According to Eqs. (3)-(5) and the different parameters of our system, a train of pulses with a repetition frequency of  $0.3\tau_{\text{ODL}}$  (ps) GHz and an approximated envelope duration of  $1.67/\tau_{\text{system}}$  (ps) ns for a TBP of 0.5 is obtained at the output of the SOA-MZI structure. The bandwidth of the generated THz radiation is expected to follow  $0.3\tau_{\text{system}}$  (ps) GHz.

The traces included in Fig. 3 were obtained in a digital communication analyzer with 30 GHz bandwidth and correspond to the points shown in Fig. 1(b). Trace 1 is for the chirped pulse at the input of the SOA-MZI while trace 2 is the shaping waveform. Trace 3 shows the XGM effect induced by the carrier saturation arising from the shaping waveform injection in the upper SOA. Traces 4a and 4b are for the SOA-MZI output without and with the shaping signal being injected, respectively. For the latter, the combined effect of XGM and XPM can be seen [20]. A slight asymmetry in the biasing currents was observed to provide a better extinction ratio for the spectral filtering. Indeed, the optimum SOAs biasing currents were found to be 110 and 100 mA for the upper and lower, respectively.

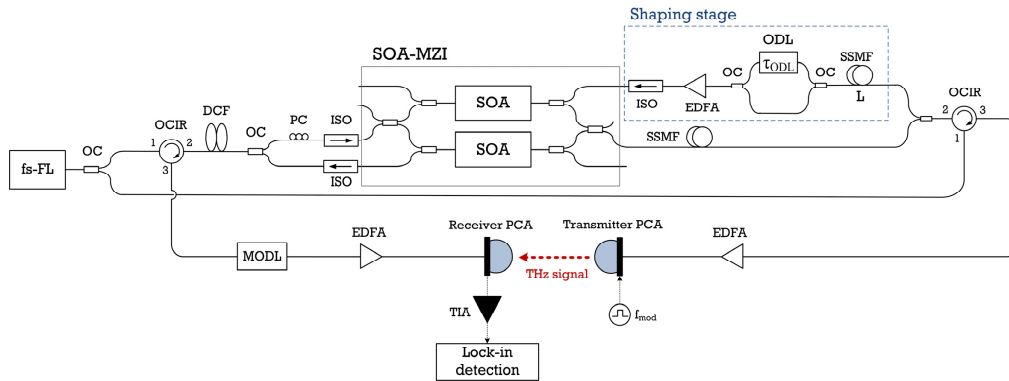


Fig. 2. Optical pulse shaper integrated in a fiber-based THz-TDS system.

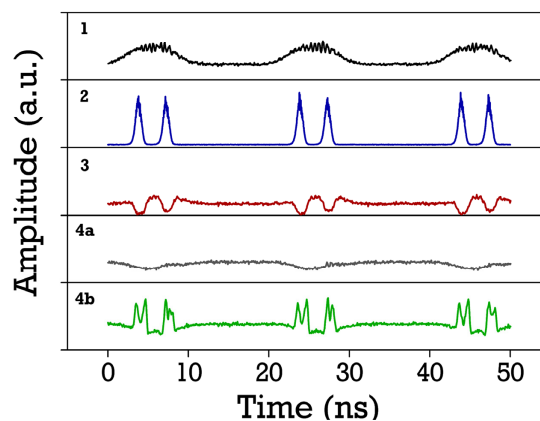


Fig. 3. Photo-detection traces at different points of the SOA-MZI structure as shown in Fig. 1(b).

After the SOA-MZI the pulse is dispersion compensated by means of 25 km of SSMF with a dispersion parameter of 16.7 ps/km-nm. Due to the need of time alignment between the transmitter and receiver branches of the THz-TDS system, compensating for possible sources of error in both branches turns out to be important. We experimentally observed how the initial difference in fiber length between the transmitter and receiver branches led to time fluctuations of the THz pulse in the order of hundreds of ps. This occurs because of fiber expansion and contraction due to temperature changes. To solve this problem the optical pulses of both transmitter and receiver pulse must travel similar distances. This is done by the use of optical couplers (OC), optical circulators (OCIR) and isolators (ISO). The 1x2 OCs employed in the system had a coupling ratio of 50/50 and a directivity of 50 dB. The insertion losses of the OCs, ISOs and OCIRs were 0.5, 0.7 and 1 dB, respectively. The ISOs and the OCIRs provided isolation larger than 40 dB. The OCIRs showed both directivity (signal from port 1 to 3) and return loss higher than 50 dB. According to these values both signal paths could be considered independent as confirmed by the experimental measurements.

A motorized optical delay line (MODL) is employed to sweep the THz traces in 100 fs steps and EDFAs to boost the optical signals into the mW range before feeding the 1.5  $\mu\text{m}$  PCAs. Lock-in detection after  $10^6$  V/A of trans-impedance amplification (TIA) is employed to record the electric field. The transmitter antenna is square biased from  $-10$  to  $+10$  V at a frequency ( $f_{\text{mod}}$ ) of 1 kHz.

Before injecting the shaped pulse into the THz system, autocorrelation traces are obtained. The central frequency and its bandwidth are controlled by means of the MZI delay and the

fiber length, respectively. In Fig. 4(a) the duration of the envelope does not change because the fiber length is kept constant and the pulse train duration is directly related to the bandwidth of the filtered spectral bands. Trains of pulses with a repetition period of 2.7, 1.64 and 1.05 ps are obtained for increasing values of  $\tau_{ODL}$  according to Eq. (3). In Fig. 4(b) a set of different values for  $L$  is considered for the same  $\tau_{ODL}$ . Fiber reels of 1, 2 and 5 km widened the optical pulses up to 200 ps, 400 ps and 1 ns, respectively, and biasing currents of 300 mA were used for the SOAs.

For comparison purposes, the THz-TDS system of Fig. 2 is tested without applying any shaping to the signal (by switching off the upper SOA). The estimated FWHM of the pulses applied to both PCAs is 300 fs, with an average power of 10 dBm and 5 dBm in the transmitter and receiver, respectively. Recovery of the original pulse duration was not possible since only the second-order dispersion was compensated. Figure 5 shows the THz trace recorded as well as its Fourier transform.

Finally, the narrowband THz-TDS system is tested in different frequency bands. Figure 6 shows the different THz waveforms and their corresponding spectra. In Fig. 6(a), as well as in Fig. 5(a), a low frequency component appears as an increasing current slope after the pulse train which is thought to originate from impedance mismatching in the antenna. In Fig. 6(b) narrowband radiation with central frequencies of 300, 550 and 700 GHz can be seen.

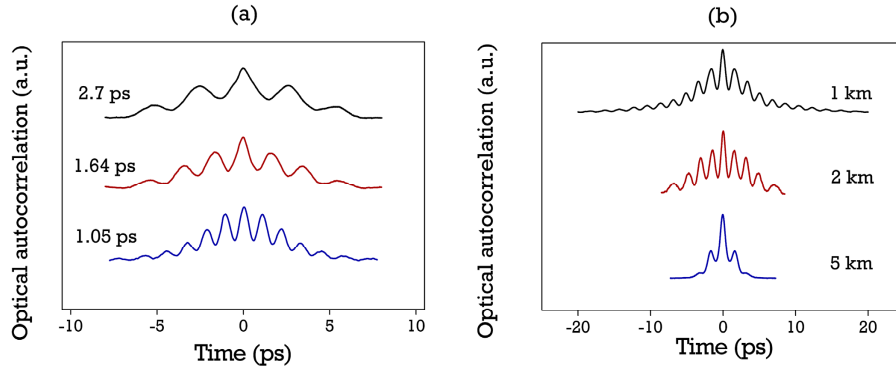


Fig. 4. Optical autocorrelation traces for several values of (a) delay and (b) fiber length in the shaping stage.

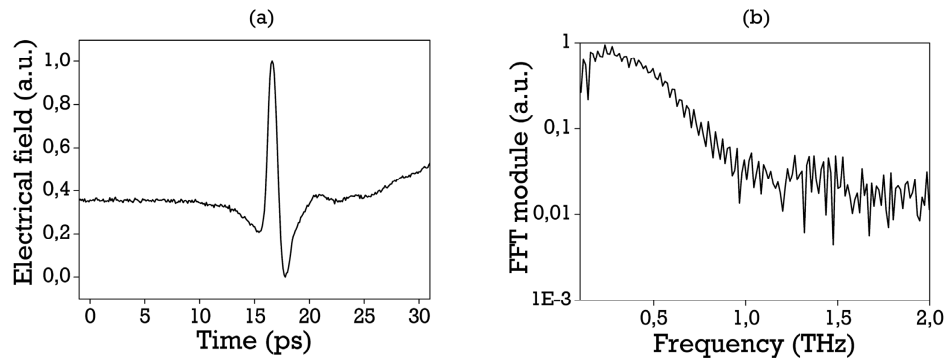


Fig. 5. (a) Time-domain THz waveform and (b) its corresponding spectra when no shaping is performed.

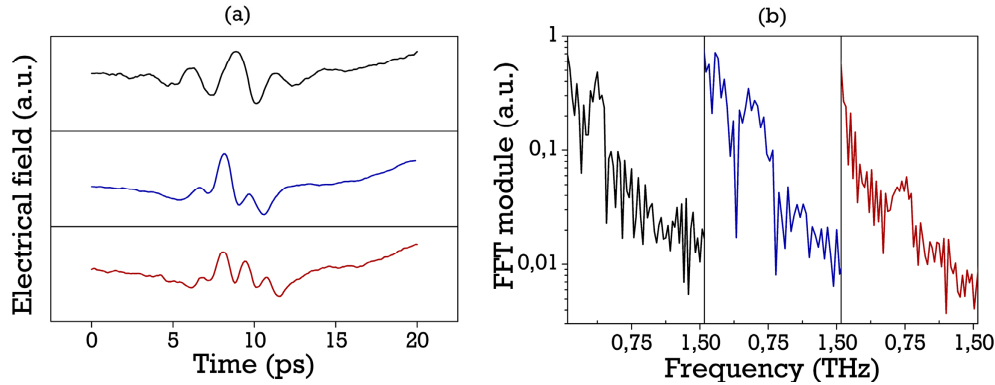


Fig. 6. (a) Time-domain THz waveforms and (b) their corresponding spectra for different frequency bands.

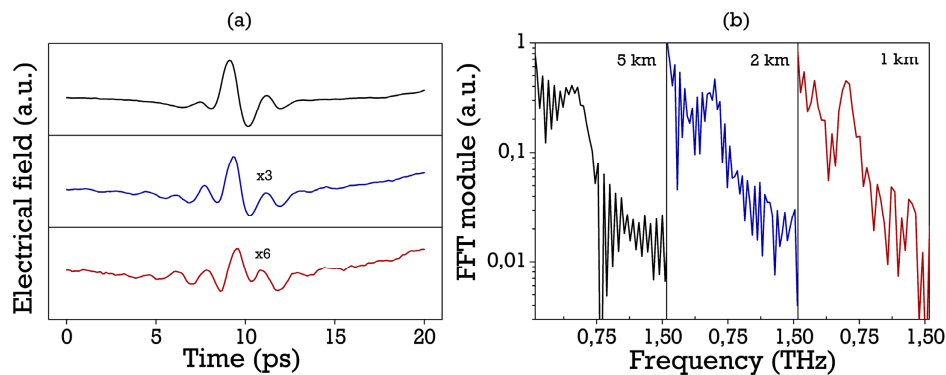


Fig. 7. (a) Time-domain THz waveforms and (b) their corresponding spectra for bandwidth reconfiguration.

After showing the tunability of the system the THz radiation bandwidth is controlled by changing the amount of fiber in the shaping stage,  $L$ . THz waveforms as well as their spectra are included in Fig. 7 where  $\tau_{ODL}$  is kept constant and the narrowing of the spectrum as the fiber length decreases can be appreciated. Low-frequency components arising from beating among components of the same spectral band are reduced for narrower THz bandwidths as shown in Fig. 7. Optical switches can be employed to select among different fiber reels. In this case the amount of fiber in the shaping stage is used to control the width of the THz radiation, although other approaches could be considered. Phase modulation has been reported to be able to compensate for the dispersion of a fiber link [21]. Therefore it could be employed to dynamically change the radiation bandwidth by increasing or reducing the accumulated dispersion. The SOA dynamics could also be controlled through its bias current or by adding a low wavelength component which would change the response time of the SOA and therefore the selected bands' bandwidth [20].

#### 4. Conclusions

An all-optical fiber based THz pulse shaping scheme based on the optical modulation of the spectrum of ultra-short pulses is proposed and demonstrated. It allows for both tunability and reconfigurability of the emitted radiation through independent system parameters as opposed to previous solutions. Additionally, since it is an all-fiber approach, compact and robust instruments can be implemented. The precision of the modulation of the pulse spectrum is given by the recovery time of the SOA and the amount of dispersion that can be introduced onto the signal. High performance could be obtained through a large linear chirping of the

signal and fast SOAs, although the introduction of non-linear dispersion could make the generation process more difficult due to the effect of the non-linear mapping of the spectrum in the time domain. The experimental measurements performed agree well with the theoretical analysis performed and prove the feasibility of dynamic THz processing systems able to concentrate the radiated energy in the spectral region of interest. Although the measurements performed show simple pulse shapes the proposed technique could provide arbitrary pulse shaping by using state-of-the-art SOAs.

### **Acknowledgments**

This work has been partially supported by the Spanish Ministerio de Economía y Competitividad (TEC2009-08078). Jesús Palaci is supported by the Formación de Personal Investigador grant program of the Universidad Politécnica de Valencia.